Progress In Electromagnetics Research M, Vol. 97, 167–176, 2020

Analysis of Surface Wave Attenuation in Double-Layer Magnetic Absorbing Sheet for Wide Frequency Range Application

Yinrui Li, Jiaji Yang, Dongmeng Li, Wei Gong, Xian Wang*, and Rongzhou Gong

Abstract—We firstly derived the simplified formulas for calculating attenuation constants of surface wave in double-layer magnetic absorbing sheets (MASs). The fabricated two kinds of magnetic absorbing sheets, having advantages in the low and high frequency range respectively, were used to design a group of 0.5 mm-thick double-layer sheets. Numerical calculation results show that the surface wave attenuation constants of double-layer absorbing sheet with a proper combination of the two MASs can be significantly enhanced in the whole frequency range, compared to those single-layer sheets of the same thickness. Furthermore, the simulations of monostatic RCS reduction of the metal slab coated with double-layer MAS well confirm the calculation analysis. This work demonstrates that it is feasible for double-layer magnetic absorbing sheet to enhance the surface wave attenuation ability and broaden application frequency range.

1. INTRODUCTION

As we all know, when the surface waves propagate to the electromagnetic discontinuities, such as edges, gaps, and steps, strong echoes contributing to the back scattering will arise, which is the main cause of non-specular scattering [1–4]. Much interest has been shown in magnetic absorbing materials (MAMs), whose main purpose is to control specular reflection meanwhile suppress non-specular scattering. By employing MAMs, the intensity of surface wave can be significantly reduced before reaching the electromagnetic discontinuities, thus the non-specular scattering can be suppressed [2–4]. Ling et al. [5] analyzed the fundamental characteristics of the TM-type surface wave in single absorbing layer including propagation and attenuation constants, electric and magnetic losses, phase and energy velocities, etc. firstly and systematically. Subsequently, the transformation of TM-type surface wave and fundamental properties of TE-type surface wave in single absorbing layer were also reported by them [6, 7]. Recently, resistive loading, impedance loading at margins and magnetic thin film loading on single-layer RAM for enhancement of surface wave attenuation were reported by Chen et al. [2, 8, 9]. However, it is very hard for a single-layer microwave absorbing sheet to realize strong attenuation of surface waves over a wide frequency range (1–18 GHz) based on the previous reports. Unfortunately, the numerical analysis of surface wave attenuation constants in two or more layers composite absorbing sheets is very complicated according to the complex transcendental relationship in the dispersion equation of surface waves. This greatly restricts the theoretical design of multilayers composite absorbing sheets to further suppress non-specular scattering in the frequency range as wide as possible.

In this work, the simplified formulas for TM-type surface wave attenuation constants in double-layer magnetic absorbing sheets were firstly deduced. Two kinds of magnetic absorbing sheets were fabricated, and their constitutive properties were analyzed. The surface wave attenuation constants of the double-layer MASs with different thickness ratios and stacking sequences of the two sheets were numerically

Received 14 May 2020, Accepted 27 September 2020, Scheduled 18 October 2020

* Corresponding author: Xian Wang (wangx@hust.edu.cn).

The authors are with the School of Optical and Electronic Information, Wuhan National Laboratory for Optoelectronics (WNLO), Huazhong University of Science and Technology, Wuhan 430074, China.

investigated, respectively. Furthermore, the simulations of monostatic RCS are conducted to validate the calculation analysis of surface wave attenuation. The results can be the theoretical guidance to explore new microwave absorbing materials to attenuate the surface waves for wide frequency range application.

2. THEORETICAL DERIVATION

To avoid the complicated transcendental relationship in the dispersion equation, we firstly derived the simplified formulas for calculating attenuation constants of surface wave in a double-layer thin magnetic absorbing sheet. As shown in Fig. 1, a double-layer thin absorbing sheet is placed on a perfectly conducting substrate in the X-Y plane, which is laminated by two composites along Z-axis with the layer thickness of h_1 (Region 1) and h_2 (Region 2), respectively. The complex permittivity and permeability of the two composites are denoted by $\varepsilon_1 = \varepsilon_1' - j\varepsilon_1''$ and $\mu_1 = \mu_1' - j\mu_1''$ in Region 1, $\varepsilon_2 = \varepsilon_2' - j\varepsilon_2''$ and $\mu_2 = \mu_2' - j\mu_2''$ in Region 2, respectively. Region 3 above the absorbing sheet is the free space or air with the vacuum permittivity ε_0 and permeability μ_0. We assume that a TM-type surface wave propagates along the X-axis, and the field quantities are independent of the coordinate Y. A time dependence $\exp(-j\omega t)$ is assumed and suppressed below.

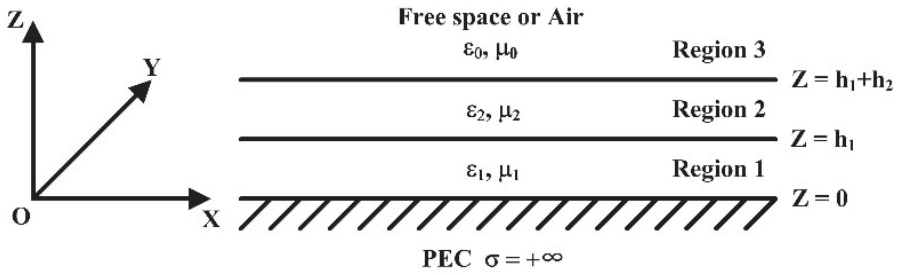

Figure 1. Schematic diagram of the double-layer absorbing sheet.

Generally, the wave number of surface wave can be regarded as the combination of transverse and longitudinal wave numbers. For the following derivation process, the quantity $\beta_x = \beta_x' - j\beta_x''$ is the propagation constant, namely the longitudinal wave number of surface wave inside and outside the absorbing sheet. Since the attenuation of EM wave in a thin absorbing sheet will not be too much, it is reasonable to ignore the tiny imaginary part of β_x in the case of $\beta_x'' \ll \beta_x'$. Meanwhile, for a thin sheet, β_x' will be very close to k_0, where k_0 is the wave number of the free space or air [2]. Accordingly, we can simplify the calculation for a thin absorbing sheet with almost no deviation if we set $\beta_x = \beta_x' = k_0 = \omega\sqrt{\varepsilon_0\mu_0}$.

Hence, the wave number k_1 in Region 1 can be expressed as

$$\vec{k}_1 = \vec{x}\beta_x' + \vec{z}\left(s_{z1}' - js_{z1}''\right) \tag{1}$$

where the quantity $s_{z1} = s_{z1}' - js_{z1}''$ is the transverse wave number of Region 1. Then

$$\vec{k}_1 \cdot \vec{k}_1 = \beta_x'^2 + s_{z1}'^2 - s_{z1}''^2 - 2js_{z1}'s_{z1}'' = k_1^2 = \omega^2\left(\varepsilon_1' - j\varepsilon_1''\right)\left(\mu_1' - j\mu_1''\right) \tag{2}$$

and the real and imaginary parts of s_{z1} can be solved from Equation (2).

$$\begin{aligned} s_{z1}' &= \frac{1}{\sqrt{2}}\left\{\begin{array}{l}\sqrt{\omega^4\left(\mu_1'\varepsilon_1'' + \mu_1''\varepsilon_1'\right)^2 + \left[\omega^2\left(\mu_1'\varepsilon_1' - \mu_1''\varepsilon_1''\right) - \beta_x'^2\right]^2} \\ + \left[\omega^2\left(\mu_1'\varepsilon_1' - \mu_1''\varepsilon_1''\right) - \beta_x'^2\right]\end{array}\right\}^{\frac{1}{2}} \\ s_{z1}'' &= \frac{1}{\sqrt{2}}\left\{\begin{array}{l}\sqrt{\omega^4\left(\mu_1'\varepsilon_1'' + \mu_1''\varepsilon_1'\right)^2 + \left[\omega^2\left(\mu_1'\varepsilon_1' - \mu_1''\varepsilon_1''\right) - \beta_x'^2\right]^2} \\ - \left[\omega^2\left(\mu_1'\varepsilon_1' - \mu_1''\varepsilon_1''\right) - \beta_x'^2\right]\end{array}\right\}^{\frac{1}{2}} \end{aligned} \tag{3}$$

Similarly, the real and imaginary parts of transverse wave number s_{z2} of Region 2 are as follows:

$$\begin{aligned} s'_{z2} &= \frac{1}{\sqrt{2}} \left\{ \begin{array}{l} \sqrt{\omega^4 \left(\mu'_2\varepsilon''_2 + \mu''_2\varepsilon'_2\right)^2 + \left[\omega^2\left(\mu'_2\varepsilon'_2 - \mu''_2\varepsilon''_2\right) - \beta'^2_x\right]^2} \\ + \left[\omega^2\left(\mu'_2\varepsilon'_2 - \mu''_2\varepsilon''_2\right) - \beta'^2_x\right] \end{array} \right\}^{\frac{1}{2}} \\ s''_{z2} &= \frac{1}{\sqrt{2}} \left\{ \begin{array}{l} \sqrt{\omega^4 \left(\mu'_2\varepsilon''_2 + \mu''_2\varepsilon'_2\right)^2 + \left[\omega^2\left(\mu'_2\varepsilon'_2 - \mu''_2\varepsilon''_2\right) - \beta'^2_x\right]^2} \\ - \left[\omega^2\left(\mu'_2\varepsilon'_2 - \mu''_2\varepsilon''_2\right) - \beta'^2_x\right] \end{array} \right\}^{\frac{1}{2}} \end{aligned} \tag{4}$$

In Region 1, the field components should satisfy the Maxwell equations and the boundary condition $E_{x1} = 0$ at $z = 0$.

$$\begin{aligned} E_{x1} &= \sin\left[\left(s'_{z1} - js''_{z1}\right) z\right] e^{-j\beta'_x x} \\ E_{z1} &= \frac{-j\beta'_x}{s'_{z1} - js''_{z1}} \cos\left[\left(s'_{z1} - js''_{z1}\right) z\right] e^{-j\beta'_x x} \\ H_{y1} &= \frac{-jw\left(\varepsilon'_1 - j\varepsilon''_1\right)}{s'_{z1} - js''_{z1}} \cos\left[\left(s'_{z1} - js''_{z1}\right) z\right] e^{-j\beta'_x x} \end{aligned} \tag{5}$$

and for Region 2, the field components are

$$\begin{aligned} E_{x2} &= \sin\left[\left(s'_{z2} - js''_{z2}\right)(z - h_1) + C\right] e^{-j\beta'_x x} \\ E_{z2} &= \frac{-j\beta'_x}{s'_{z2} - js''_{z2}} \cos\left[\left(s'_{z2} - js''_{z2}\right)(z - h_1) + C\right] e^{-j\beta'_x x} \\ H_{y2} &= \frac{-j\omega\left(\varepsilon'_2 - j\varepsilon''_2\right)}{s'_{z2} - js''_{z2}} \cos\left[\left(s'_{z2} - js''_{z2}\right)(z - h_1) + C\right] e^{-j\beta'_x x} \end{aligned} \tag{6}$$

At the layer interface $z = h_1$, E_x, and H_y should satisfy their continuities, thus the factor C can be obtained.

$$C = \arctan\left\{\frac{s'_{z1} - js''_{z1}}{s'_{z2} - js''_{z2}} \cdot \frac{\varepsilon'_2 - j\varepsilon''_2}{\varepsilon'_1 - j\varepsilon''_1} \cdot \tan\left[\left(s'_{z1} - js''_{z1}\right) h_1\right]\right\} \tag{7}$$

The suitable wave equations for free space or air that satisfies the boundary condition $E_{x3} = E_{z3} = H_{y3} = 0$ when $z \to +\infty$ are

$$\begin{aligned} E_{x3} &= Ae^{-\left(s'_{z3} - js''_{z3}\right)(z - h_1 - h_2)} \cdot e^{-j\beta'_x x} \\ E_{z3} &= A\frac{-j\beta'_x}{s'_{z3} - js''_{z3}} e^{-\left(s'_{z3} - js''_{z3}\right)(z - h_1 - h_2)} \cdot e^{-j\beta'_x x} \\ H_{y3} &= A\frac{-j\omega\varepsilon_0}{s'_{z3} - js''_{z3}} e^{-\left(s'_{z3} - js''_{z3}\right)(z - h_1 - h_2)} \cdot e^{-j\beta'_x x} \end{aligned} \tag{8}$$

Similarly, at the interface $z = h_1 + h_2$, E_x and H_y should satisfy their continuities, thus the parameter A and transverse wave number s_{z3} can be got.

$$A = \sin\left[\left(s'_{z2} - js''_{z2}\right) h_2 + C\right] \tag{9}$$

$$s'_{z3} - js''_{z3} = \frac{\varepsilon_0\left(s'_{z2} - js''_{z2}\right)}{\varepsilon'_2 - j\varepsilon''_2} \tan\left[\left(s'_{z2} - js''_{z2}\right) h_2 + C\right] \tag{10}$$

The amplitudes of electric and magnetic fields in the X direction outside and inside absorbing sheet decay with the same factor $e^{-\beta''_x x}$ in order to satisfy the boundary conditions. Most of the surface wave energy is in free space or air, and by contrast, only a small part is in the absorbing sheet. As a result, the surface wave can be effectively attenuated only when the energy in the free space or air continuously enters the absorbing sheet and is absorbed. The term of $e^{js''_{z3}z}$ in Equation (8), indicating a component propagating in the $-Z$ direction, describes the surface wave energy propagation from free space into the absorbing sheet.

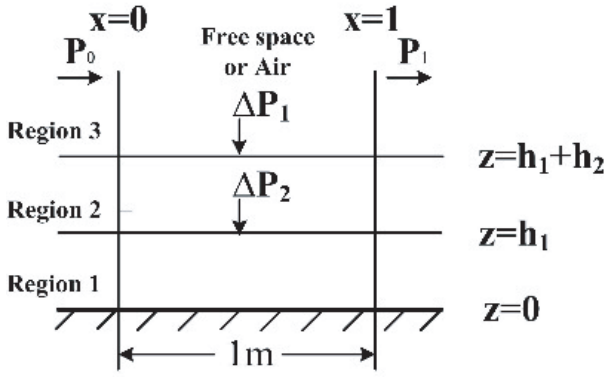

Figure 2. Model of surface wave energy loss in double-layer absorbing sheet.

We next analyzed the energy loss of surface wave in the propagation direction. Suppose that there are two planes $x = 0$ and $x = 1$, i.e., 1 meter apart along X-axis, as shown in Fig. 2. All the quantities relate to the cross section of the guiding structure with the unit width ($0 \le y \le 1$), and they are averaged in time for the period of the field oscillations. The powers through these two planes are $P_0(x = 0)$ and $P_1(x = 1)$, respectively, and the basic correlation is $P_1 = P_0 - (\Delta P_1 + \Delta P_2)$. $\Delta P_1 + \Delta P_2$ is the energy reduction between two planes; ΔP_1 is the energy loss from air through the unit surface into the Region 2; and ΔP_2 is the energy absorbed and attenuated by the Region 1 from air via the unit interface of the Region 1 and Region 2. ΔP_1 and ΔP_2 are

$$\Delta P_1 = \int_0^1 \frac{1}{2} Re\left(E_x H_y^*\right)_{z=h_1+h_2} dx \tag{11}$$

$$\Delta P_2 = \int_0^1 \frac{1}{2} Re\left(E_x H_y^*\right)_{z=h_1} dx \tag{12}$$

When calculating ΔP_1 and ΔP_2, we must consider the amplitudes decay in the X direction, so the term $e^{-\beta_x'' x}$ should be added into the field components. Then, substituting the field components into Equation (11) leads to the following explicit expression

$$\Delta P_1 = \frac{\omega}{4\left(s_{z2}'^2 + s_{z2}''^2\right)} \left[\begin{array}{l} \left(\varepsilon_2' s_{z2}'' - \varepsilon_2'' s_{z2}'\right) \sin 2\left(s_{z2}' h_2 + C'\right) \\ + \left(\varepsilon_2' s_{z2}' + \varepsilon_2'' s_{z2}''\right) \sinh 2\left(s_{z2}'' h_2 + C''\right) \end{array} \right] \cdot \frac{1 - e^{-2\beta_x''}}{2\beta_x''} = Q_1 \cdot \frac{1 - e^{-2\beta_x''}}{2\beta_x''} \tag{13}$$

where

$$Q_1 = \frac{\omega}{4\left(s_{z2}'^2 + s_{z2}''^2\right)} \left[\left(\varepsilon_2' s_{z2}'' - \varepsilon_2'' s_{z2}'\right) \sin 2\left(s_{z2}' h_2 + C'\right) + \left(\varepsilon_2' s_{z2}' + \varepsilon_2'' s_{z2}''\right) \sinh 2\left(s_{z2}'' h_2 + C''\right)\right] \tag{14}$$

In the same way, the explicit expression of ΔP_2 is

$$\Delta P_2 = \frac{\omega}{4\left(s_{z1}'^2 + s_{z1}''^2\right)} \left[\begin{array}{l} \left(\varepsilon_1' s_{z1}'' - \varepsilon_1'' s_{z1}'\right) \sin\left(2 s_{z1}' h_1\right) \\ + \left(\varepsilon_1' s_{z1}' + \varepsilon_1'' s_{z1}''\right) \sinh\left(2 s_{z1}'' h_1\right) \end{array} \right] \cdot \frac{1 - e^{-2\beta_x''}}{2\beta_x''} = Q_2 \cdot \frac{1 - e^{-2\beta_x''}}{2\beta_x''} \tag{15}$$

where

$$Q_2 = \frac{\omega}{4\left(s_{z1}'^2 + s_{z1}''^2\right)} \left[\left(\varepsilon_1' s_{z1}'' - \varepsilon_1'' s_{z1}'\right) \sin\left(2 s_{z1}' h_1\right) + \left(\varepsilon_1' s_{z1}' + \varepsilon_1'' s_{z1}''\right) \sinh\left(2 s_{z1}'' h_1\right)\right] \tag{16}$$

P_0 is the total energy transferred by the surface wave, and

$$\begin{aligned} P_0 &= \frac{1}{2} Re\left[\int_0^{h_1} E_{z1} H_{y1}^* dz + \int_{h_1}^{h_1+h_2} E_{z2} H_{y2}^* dz + \int_{h_1+h_2}^{+\infty} E_{z3} H_{y3}^* dz\right]_{x=0} \\ &= \frac{\beta_x' \omega \varepsilon_1'}{8\left(s_{z1}'^2 + s_{z1}''^2\right)} \cdot \left[\frac{\sinh\left(2 s_{z1}'' h_1\right)}{s_{z1}''} + \frac{\sin\left(2 s_{z1}' h_1\right)}{s_{z1}'}\right] \end{aligned}$$

$$+\frac{\beta'_x\omega\varepsilon'_2}{8\left(s'^2_{z2}+s''^2_{z2}\right)}\left[\frac{\sin\left[2\left(s'_{z2}h+C'\right)\right]-\sin\left[2C'\right]}{s'_{z2}}+\frac{\sinh\left[2\left(s''_{z2}h+C''\right)\right]-\sinh\left[2C''\right]}{s''_{z2}}\right]$$
$$+\frac{\omega\varepsilon_0\beta'_x}{8s'_{z3}\left(s'^2_{z3}+js''^2_{z3}\right)}\left[\cosh\left(2\left(s''_{z2}h_2+C''\right)\right)-\cos\left(2\left(s'_{z2}h_2+C'\right)\right)\right] \quad (17)$$

Accordingly,

$$P_1=P_0-(\Delta P_1+\Delta P_2)=P_0e^{-2\beta''_x}\Rightarrow P_0-(Q_1+Q_2)\frac{1-e^{-2\beta''_x}}{2\beta''_x}=P_0e^{-2\beta''_x} \quad (18)$$

Finally, the surface wave attenuation constant β''_x in double-layer thin absorbing sheet can be obtained.

$$\beta''_x=\frac{1}{2}\frac{(Q_1+Q_2)}{P_0}\ (\text{neper/m})=4.34\frac{(Q_1+Q_2)}{P_0}\ (\text{dB/m}) \quad (19)$$

3. CONSTITUTIVE PROPERTIES OF MAGNETIC ABSORBING SHEETS

Soft magnetic FeCo alloy flakes (the mass fraction of cobalt is 10%) and carbonyl iron powders (CIPs) were used as microwave absorbers. The morphologies of the absorbers were observed by a TESCAN Vega 3 SBU scanning electron microscopy (SEM), and then the magnetic hysteresis loops were measured using a Lakeshore 7404 vibrating sample magnetometer (VSM). As shown in Fig. 3, it is seen that the flake shape FeCo alloy particles exhibit a broad size distribution ranging from several to dozens of microns. The saturation magnetization (Ms) and coercivity (Hc) of the FeCo flakes are 189.9 emu/g and 38.9 Oe, respectively. On the other hand, the CIPs are composed of spherical particles with diameters of submicron to several microns, and the saturation magnetization and coercivity are 205.8 emu/g and

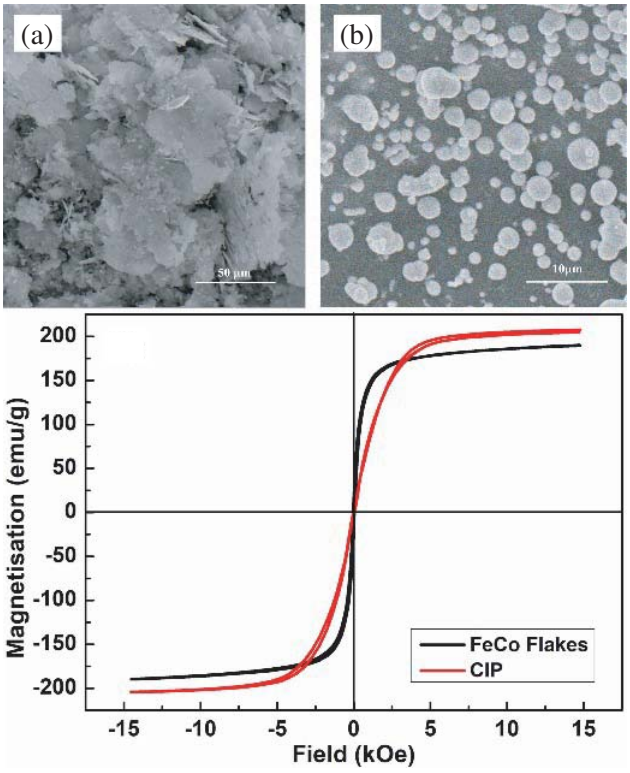

(c)

Figure 3. SEM micrographs of (a) FeCo alloy flakes and (b) CIP, (c) magnetic hysteresis loops of the absorbers.

5.9 Oe, respectively. The obvious differences in morphology and static magnetic properties between the two absorbers are favorable to produce two kinds of magnetic absorbing sheets with distinctly different microwave electromagnetic performances.

Then, magnetic absorbing sheets were fabricated by rolling process, i.e., calendaring FeCo flakes and CIP into acrylonitrile-butadiene rubber (NBR) with the mass fraction of 85%, which were named as sheet A and sheet B, respectively. The toroidal shape samples of two absorbing sheets with an outer diameter of 7 mm and an inner diameter of 3.04 mm respectively were prepared for coaxial line microwave measurements by using an Agilent N5244A PNA-X network analyzer over 0.3–18 GHz. The frequency dependency of the real and imaginary parts of complex permittivity and permeability of the two absorbing sheets are presented in Fig. 4. It is found that sheet A has obvious higher values of ε' and ε'' than those of sheet B due to the strong space-charge polarization between FeCo flakes with large surface area [10]. Moreover, both the magnetic absorbing sheets exhibit large μ' and μ'' at microwave frequencies owing to their large M_s [11, 12].

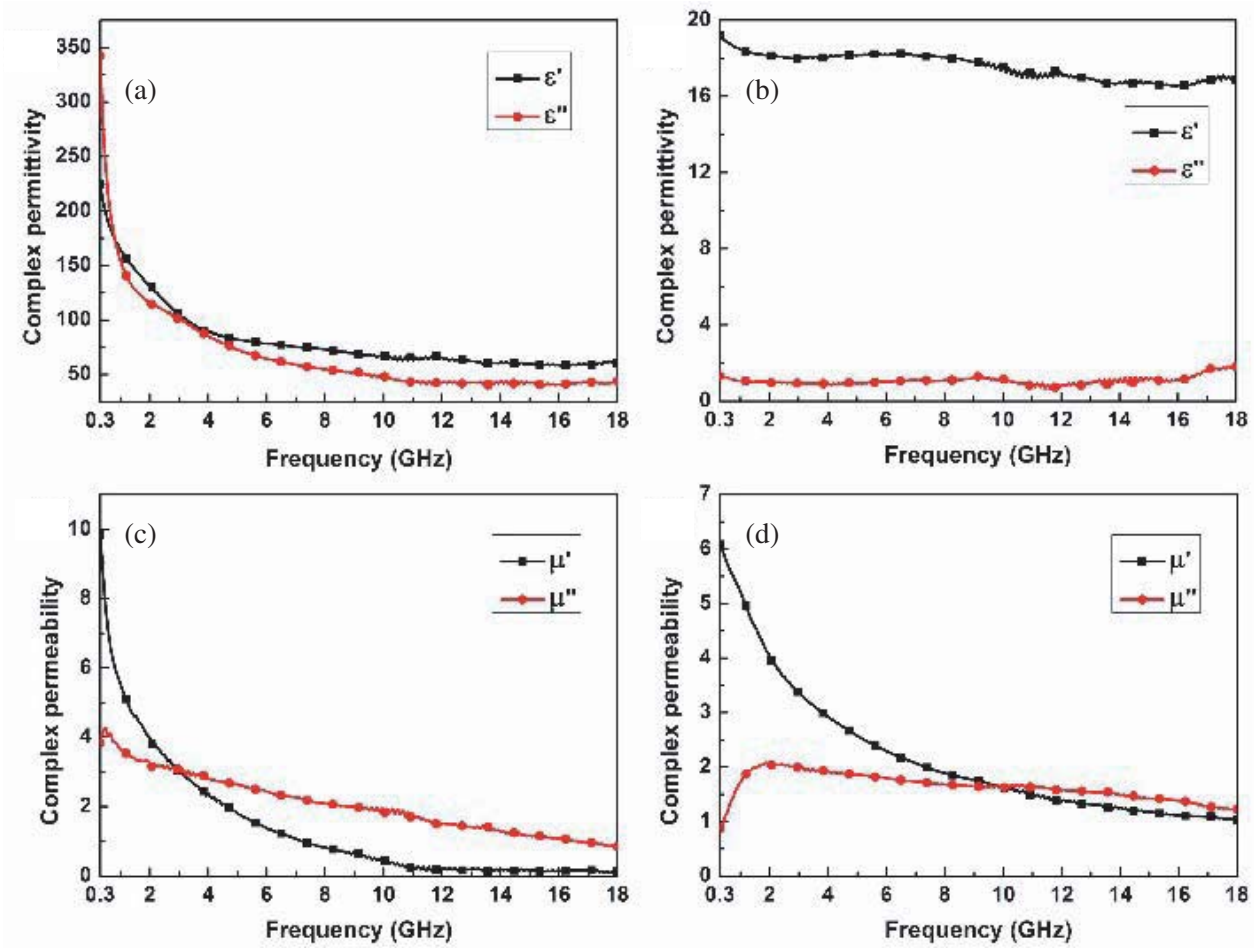

Figure 4. Complex permittivity and permeability of the magnetic absorbing sheets: (a) and (c) sheet A; (b) and (d) sheet B.

4. RESULTS AND DISCUSSION

According to the calculation method of single-layer magnetic absorbing material [2, 13], the surface wave attenuation characteristics of the above sheet A and sheet B with thicknesses of 0.2–0.5 mm were investigated, respectively. As shown in Fig. 5(a), it is seen that the attenuation constants of sheet A firstly increase then decrease with the further increase of the frequency. More interestingly, the

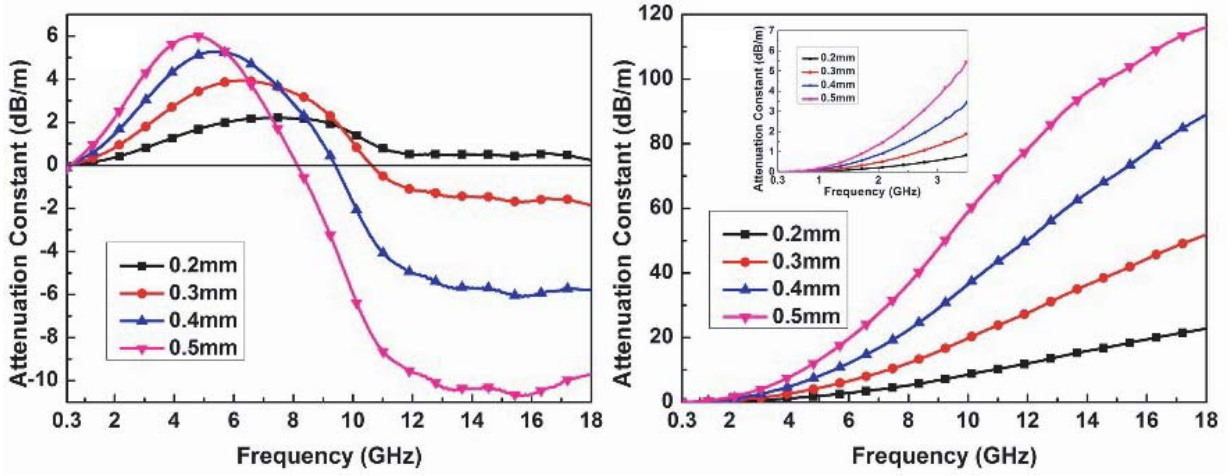

Figure 5. The calculated surface wave attenuation constants for single layer sheet with different thickness: (a) sheet A, (b) sheet B.

maximum attenuation constant increases, but the upper cutoff frequency shifts to lower frequency with thicker thickness. The negative attenuation constants beyond upper cutoff frequency can be interpreted as follows. Surface waves cannot be excited and propagate along the absorbing sheet, and transform into "non-physical waves" [5, 6]. In other words, the magnetic absorbing sheet can only play a role in energy loss when the frequency of surface wave is lower than upper cutoff frequency. In Fig. 5(b), the attenuation constants of sheet B increase monotonously with the increase of the frequency and thickness. This indicates that the upper cutoff frequency of sheet B exceeds 18 GHz even at the thickness of 0.5 mm. It is noteworthy that sheet B exhibits significantly large attenuation constants in higher frequency field (over the operating frequency range of sheet A), but is smaller than those of sheet A at the same thickness within low frequency band, as illustrated in set of Fig. 5(b). In comparison, sheet A is more suitable for attenuating the low-frequency surface waves, while sheet B has better absorption efficiency for high-frequency surface waves. Thus, we can qualitatively define sheet A as the "low-frequency loss sheet" and sheet B as the "high-frequency loss sheet", respectively. A proper combination of sheet A and B may be beneficial for improving surface wave attenuation in wide frequency range by taking advantage of the strengths of both sheets.

Furthermore, we focus on the surface wave attenuation performances of the double-layer sheet composed of magnetic absorbing sheet A and sheet B according to the above deduced calculation formulas. The attenuation constants of a group of 0.5 mm-thick double-layer absorbing sheets with different thickness ratios of the upper (Region 2, R2) and lower (Region 1, R1) layers are shown in Fig. 6. For the first case, in Fig. 6(a), low-frequency loss sheet A is in layer R1, and high-frequency loss sheet B is in layer R2. The thickness of sheet A is increased in the steps of 0.1 mm, while sheet B is decreased synchronously when the total thickness is kept at 0.5 mm. As a result, it is observed that the attenuation constants of double-layer sheet show a continuous increase in the low frequency range with the increasing thickness of sheet A. However, the attenuation constants in the high frequency range firstly increase and then decline gradually when the thickness of sheet A is larger than 0.3 mm. This can be ascribed to the red shift of the upper cutoff frequency of sheet A with increasing thickness, i.e., too thick low-frequency loss sheet A is not conducive to attenuate high-frequency surface waves. In comparison, the double-layer absorbing sheet labeled as 0.2 mm R1(A)–0.3 mm R2(B) shows the largest values of attenuation constant in the high frequency range with enhancement in the low frequency range. In Fig. 6(b), the second case is the stacking sequence of sheet A, and sheet B is exchanged. As the thickness of sheet A is increased, the attenuation constant drastically decreases in the high frequency region; meanwhile, the upper cutoff frequency shifts to the lower frequency. This phenomenon can be explained as follows: the thicker sheet A with high complex permittivity as the top layer makes the longitudinal surface impedance of the TM-type surface wave change into capacitive at lower frequencies, and thus the upper

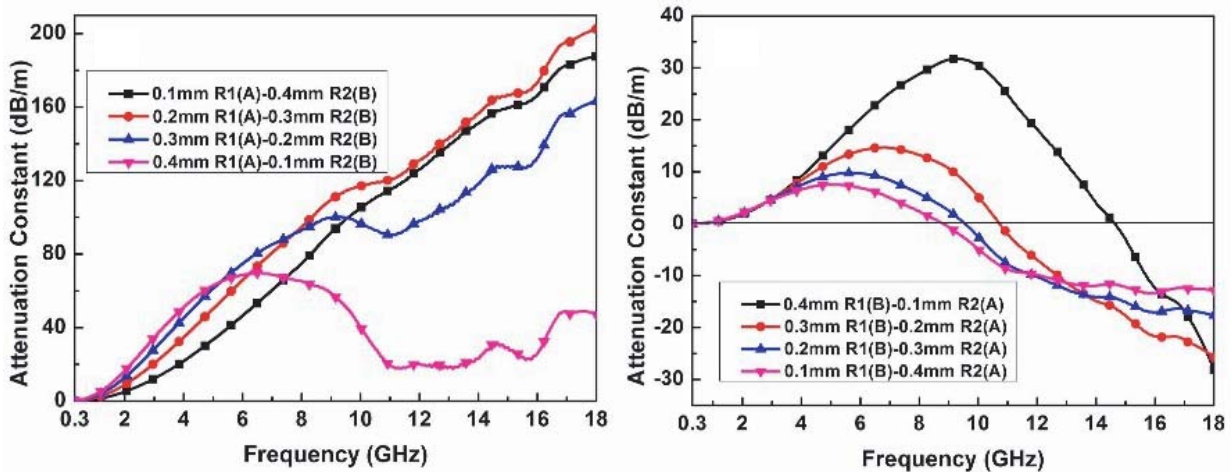

Figure 6. The calculated attenuation constants of 0.5 mm-thick double-layer magnetic absorbing sheets composed of sheet A and sheet B with different thickness ratios. (a) Sheet A is in Region 1, sheet B is in Region 2; (b) Sheet B is in Region 1, sheet A is in Region 2.

cutoff frequency appears earlier [2, 4, 5]. So it is crucial to optimize the electromagnetic parameters of surface layers for broadband surface wave attenuation. Overall, a proper combination of sheet A and sheet B can effectively improve attenuation constants in the wide frequency, as listed in Table 1. The results suggest that double-layer magnetic absorbing sheets have an advantage over single-layer sheets for non-specular scattering suppression due to their enhanced surface wave attenuation ability.

Table 1. Typical values of attenuation constants for single layer sheets and double-layer sheets at the thickness of 0.5 mm.

Frequency (GHz)	Attenuation constant (dB/m)			
	sheet A	sheet B	0.2 mm R1(A)–0.3 mm R2(B)	0.3 mm R1(B)–0.2 mm R2(A)
2	2.12	1.34	9.43	2.08
4	5.98	7.66	35.20	8.44
8	0.55	36.33	95.47	13.24
15	−10.01	102.77	166.47	−17.63

In order to validate the above calculation analysis of surface wave attenuation, the mono-static RCS reduction of a metal slab coated with the magnetic absorbing sheets was further studied using time domain solver in EM simulation software of CST MICROWAVE STUDIO. The metal slab is made of copper with the dimension 500 × 100 × 0.035 mm. It is noticeable that the slab is thin enough so as to avoid edge scattering and exceeds the skin depth. The mono-static RCS simulations of the metal slabs uncoated and coated with magnetic absorbing sheet were performed under the horizontal (HH) polarization plane wave at the frequencies of 2 GHz, 4 GHz, 8 GHz, and 15 GHz, respectively, as shown in Fig. 7. It can be observed that there is a significant reduction in the RCS of the metal slab after coating three types of absorbing materials, i.e., 0.5 mm-thick single-layer of sheet A, sheet B, and the double-layer absorbing sheet of 0.2 mm R1(A)–0.3 mm R2(B), respectively. When the incident angle is in the range of 0–70°, the launching efficiency of surface wave is less than 10% for all the cases [5]. So the surface wave attenuation abilities of the magnetic absorbing sheets are generally evaluated according to the RCS reductions, i.e. the difference of the peak values at the incident angle of around 75° before

coating and after coating respectively [13, 14]. The reduction of RCS, listed in Table 2, is in good agreement with the magnitude of surface wave attenuation constants. In other words, with the same thickness, the RCS reduction at 2 GHz of metal slab coated with low-frequency loss sheet A is larger than that with high-frequency loss sheet B, but opposite at the high frequencies of 4 GHz, 8 GHz, and 15 GHz. As expected, the double-layer sheet shows greater RCS reduction than that of the two single-layer sheets in the whole frequency range.

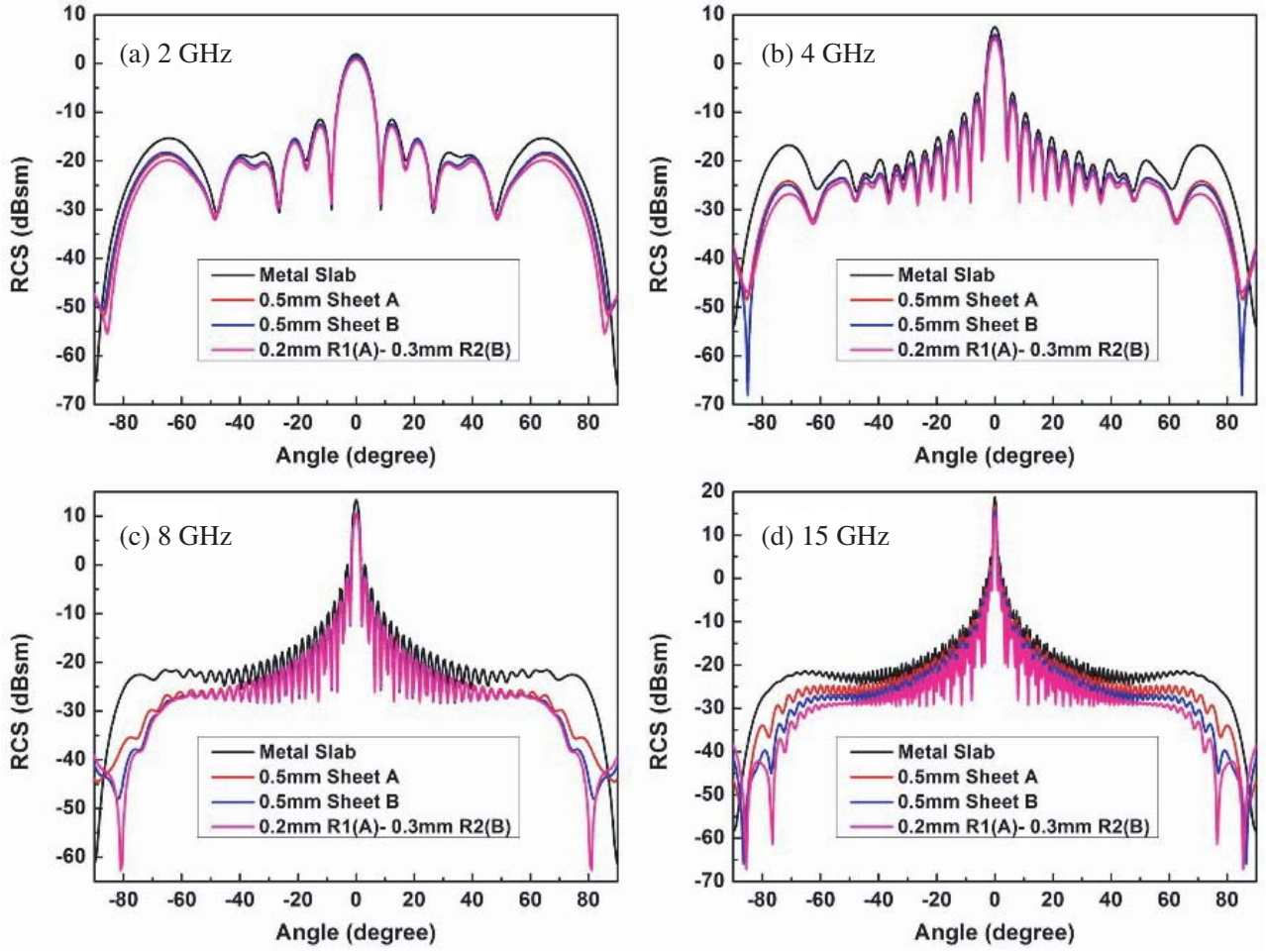

Figure 7. HH-polarization mono-static RCS diagrams for metal slab uncoated and coated with magnetic absorbing sheets at (a) 2 GHz, (b) 4 GHz, (c) 8 GHz and (d)15 GHz, respectively.

Table 2. The RCS reduction values at four typical frequencies.

Frequency (GHz)	RCS reduction (dBsm)		
	sheet A	Sheet B	0.2 mm R1(A)–0.3 mm R2(B)
2	3.39	2.97	4.5
4	7.39	8.1	10.02
8	12.85	15.34	15.85
15	7.89	13.66	16.18

5. CONCLUSION

In summary, we have investigated the performance of surface wave attenuation in double-layer magnetic absorbing sheets through numerical calculation and simulation. According to our deduced simplified formulas, it is found that the surface wave attenuation constants can be effectively manipulated by changing the thickness ratios and stacking sequences of the two magnetic absorbing sheets, i.e., low-frequency loss sheet A and high-frequency loss sheet B. In comparison with single-layer sheets at the same thickness of 0.5 mm, the double-layer absorbing sheet 0.2 mm R1(A)–0.3 mm R2(B) shows significant larger values of attenuation constants in the whole frequency range. Furthermore, the simulation results verify that the double-layer absorbing sheet with such a proper combination of the two sheets is more efficient to obtain the reduction of RCS due to its relatively strong surface wave attenuation ability. The present work provides a pathway to develop better magnetic absorbing materials for surface wave attenuation over wide frequency range.

REFERENCES

1. Chen, H.-Y., L.-J. Lu, D.-J. Guo, H.-P. Lu, P.-H. Zhou, J.-L. Xie, and L.-J. Deng, "Relationships between surface wave attenuation and the reflection properties of thin surface wave absorbing layer," *PIERS Proceedings*, 1146–1150, Guangzhou, China, August 25–28, 2014.
2. Li, Y., D. Li, X. Wang, et al., "Influence of the electromagnetic parameters on the surface wave attenuation in thin absorbing layers," *AIP Adv.*, Vol. 8, No. 5, 056616, 2018.
3. Chen, H. Y., H. P. Lu, J. L. Xie, et al., "Improvement of surface waves attenuation performance with a magnetic thin film loading," *IEEE Trans. Magn.*, Vol. 50, No. 7, 1–5, 2014.
4. Stroobandt, S., "The characterization of surface waves on low-observable structures," Master's thesis, Univ. of Hull, 1997.
5. Ling, R. T., J. D. Scholler, and P. Ya. Ufimtsev, "The propagation and excitation of surface waves in an absorbing layer," *Progress In Electromagnetics Research*, Vol. 19, 49–91, 1998.
6. Ufimtsev, P. Y., R. T. Ling, and J. D. Scholler, "Transformation of surface waves in homogeneous absorbing layers," *IEEE Trans. Antennas Propag.*, Vol. 48, No. 2, 214–222, 2000.
7. Ufimtsev, P. Y. and R. T. Ling, "New results for the properties of TE surface waves in absorbing layers," *IEEE Trans. Antennas Propag.*, Vol. 49, No. 10, 1445–1452, 2001.
8. Chen, H.-Y., L.-J. Deng, P.-H. Zhou, J. Xie, and Z.-W. Zhu, "Improvement of surface electromagnetic waves attenuation with resistive loading," *Progress In Electromagnetics Research Letters*, Vol. 26, 143–152, 2011.
9. Chen, H. Y., L. J. Deng, and P. H. Zhou, "Suppression of surface wave from finite conducting surfaces with impedance loading at margins," *Journal of Electromagnetic Waves and Applications*, Vol. 24, No. 14–15, 1977–1989, 2010.
10. Liu, J., M. Itoh, M. Terada, et al., "Enhanced electromagnetic wave absorption properties of Fe nanowires in gigaherz range," *Appl. Phys. Lett.*, Vol. 91, No. 9, 093101, 2007.
11. Wang, X., Q. Li, Z. Su, et al., "Enhanced microwave absorption of multiferroic Co_2Z hexaferrite-$BaTiO_3$ composites with tunable impedance matching," *J. Alloy. Compd.*, Vol. 643, 111–115, 2015.
12. Ye, J., Y. Liu, X. Chen, et al., "Microwave electromagnetic and absorption properties of SmN/α-Fe/$Sm_2Fe_{17}N_3$ composites in 0.5–18 GHz range," *J. Alloy. Compd.*, Vol. 526, 59–62, 2012.
13. Li, Y., D. Li, H. Luo, et al., "Co-evaluation of reflection loss and surface wave attenuation for magnetic absorbing material," *IEEE Trans. Antennas Propag.*, Vol. 66, No. 11, 6057–6060, 2018.
14. Chen, H.-Y., P.-H. Zhou, L. Chen, and L.-J. Deng, "Study on the properties of surface waves in coated RAM layers and monostatic RCSR performances of the coated slab," *Progress In Electromagnetics Research M*, Vol. 11, 123–135, 2010.